Bending of flexible magnetic rods

A. Cēbers*
Institute of Physics, University of Latvia, Salaspils-1, LV-2169, Latvia

I. Javaitis
Faculty of Physics and Mathematics, University of Latvia, Zellu 8, Riga, LV-1002, Latvia
(Received 5 March 2004; published 26 August 2004)

The flexible inextensible magnetic rod model is applied for the study of bending and buckling deformations of the paramagnetic particle chains linked by polymer molecules. It is shown that the existing experimental results can be reasonably well described by this model which takes into account the normal magnetic forces arising at chain bending deformation. By matching the experimentally observed shapes with our numerical simulation results different physical properties of the linked paramagnetic particle chains are determined.

DOI: 10.1103/PhysRevE.70.021404 PACS number(s): 82.70.Dd, 83.80.Gv, 47.65.+a

I. INTRODUCTION

Flexible magnetic rods have been of great interest recently [1–6]. It has been shown that flexible magnetic rods may be employed as micromechanical sensors for probing rigidity at molecular scale [5]. The bending rigidity of the chains of magnetic particles linked by polymers was measured recently by applying deformation to the rod by laser tweezers [6]. In respect of the obtained results it should be mentioned that the curvature elasticity constants which were determined in different sets of experiments—bending of the rod and buckling of the rod under the compressional stress, differ considerably—more than three times. As we illustrate in the present paper, it can be interpreted by the action of the magnetic force normal to the rod. To account for this force we interpret the micromechanical data of the rod micromanipulation by the model of inextensible flexible magnetic rod developed in Ref. [7]. By this model it was found that hairpin shapes of the rod are possible under the action of the field [7]. This finding has been recently confirmed experimentally [5]. In the present paper we are studying the influence of magnetic field on the dynamics and statics of the flexible magnetic rod. We are able to describe by our model the shapes observed in the bending and buckling experiments of Ref. [6] and describe the relaxation dynamics of the magnetic particle chains observed in this work. By matching the experimentally observed rod shapes under the action of the applied force and magnetic field we have found the magnetic permeability of the linked magnetic particles which have a sandwichlike structure [6]. The model of the flexible magnetic rod and some analytical results concerning the dynamics of the rod are given in Sec. II. Numerical simulation results and their comparison with available experimental data are given in Sec. III.

II. MODEL

The model of the flexible magnetic rod is developed in Ref. [7]. It is based on the Kirchhoff model of an elastic rod [8] extended by inclusion of the magnetic energy term to the total energy of the rod:

$$E = \frac{1}{2}C\int \frac{1}{R^2}dl - \frac{2\pi^2 a^2 \chi^2 H_0^2}{\mu+1}\int (\vec{h}\cdot\vec{t})^2 dl - \int \Lambda dl. \quad (1)$$

Here R is the radius of the curvature of the centerline of the rod, C is the curvature elasticity constant, a is the radius of the rod considered as the cylinder, χ is the magnetic susceptibility $\mu=1+4\pi\chi$, $\vec{t}$ is the unit vector parallel to tangent of the centerline and is given by its components $(\cos\vartheta, \sin\vartheta)$, and the Lagrange multiplier Λ accounts for the local inextensibility of the rod. Considering the variation of Eq. (1) at the variation of the position of the centerline $\vec{r}'=\vec{r}+\vec{\xi}$ we have

$$\delta E = [M\delta\varphi] + [F_t\xi_t] + [F_n\xi_n] - \int K_n\xi_n dl - \int K_t\xi_t dl. \quad (2)$$

Here, [ ] denotes the terms at the ends of the rod, ξ_n and ξ_t are the components of the Lagrange displacement in the directions of the normal and tangent to the centerline, respectively, but $\delta\varphi=\partial\xi_n/\partial l-\xi_t/R$ is the angle of tangent rotation at the Lagrange displacements $\vec{\xi}$. Tangent and normal vectors are connected according to the Frenet equation $d\vec{t}/dl=-1/R\vec{n}$. Binormal is defined by $\vec{b}=[\vec{t}\times\vec{n}]$. According to relation (2), the following expressions for the components of the body force $\vec{K}$, stresses $\vec{F}$, and momentum stresses $\vec{M}=M\vec{b}$ are valid

$$F_n = C\left(\frac{1}{R}\right)_l + \frac{2\pi^2 a^2\chi^2 H_0^2}{\mu+1}\sin 2\vartheta, \quad (3)$$

$$F_t = -\left(\frac{C}{2R^2}+\Lambda\right), \quad (4)$$

*Email address: aceb@tesla.sal.lv

$$K_n = \frac{dF_n}{dl} - \frac{F_t}{R} = C\left[\left(\frac{1}{R}\right)_{ll} + \frac{1}{2}\frac{1}{R^3}\right] + \Lambda\frac{1}{R} + \frac{2\pi^2 a^2 \chi^2 H_0^2}{\mu+1}\frac{d}{dl}\sin 2\vartheta, \tag{5}$$

$$K_t = \frac{dF_t}{dl} + \frac{F_n}{R} = -\Lambda_l + \frac{1}{R}\frac{2\pi^2 a^2 \chi^2 H_0^2}{\mu+1}\sin(2\theta), \tag{6}$$

$$M = -C/R. \tag{7}$$

As can be seen from the relations (3)–(7), in the magnetic field additional force $F_n' = [2\pi^2 a^2 \chi^2 H_0^2 \sin(2\vartheta)]/\mu+1$ normal to the rod appears as required by the momentum balance

$$\frac{d\vec{M}}{dl} + [\vec{t}\times\vec{F}] + \vec{T}_0 = \vec{0}, \tag{8}$$

where $\vec{T}_0 = -[2\pi\chi^2 H_0^2 \sin(2\vartheta)\pi a^2]/\mu+1\vec{b}$ is the torque per unit length due to the applied field.

In the simplest case of the Rouse dynamics [9] for the velocity of the centerline we have

$$\zeta\vec{v} = \vec{K}.$$

Here ζ is the friction coefficient of the chain per unit length. Accounting for the inextensibility of the rod

$$\frac{\partial v_t}{\partial l} + v_n\frac{1}{R} = 0 \tag{9}$$

and the relation for the tangent angle change [7]

$$\frac{\partial\vartheta}{\partial t} = \frac{\partial v_n}{\partial l} - \frac{v_t}{R}, \tag{10}$$

the following set of dimensionless equations for the tangent angle ϑ and tension in the rod Λ are obtained:

$$\vartheta_t = -\left(\vartheta_{llll} + \frac{1}{2}(\vartheta_l^3)_l\right) - (\theta_l\Lambda)_l - \Lambda_l\vartheta_l + \mathrm{Cm}[\sin(2\vartheta)]_{ll} - \mathrm{Cm}(\vartheta_l)^2\sin 2\vartheta, \tag{11}$$

$$\theta_l^2\Lambda - \Lambda_{ll} = -\vartheta_l\left(\vartheta_{lll} + \frac{1}{2}\vartheta_l^3\right) + \mathrm{Cm}\ \vartheta_l^2 2\cos(2\vartheta) + \mathrm{Cm}[\vartheta_l\sin(2\vartheta)]_l. \tag{12}$$

Here the dimensionless variables are introduced scaling the length with L ($2L$ is the length of the rod), time with $\zeta L^4/C$. The magnetoelastic number characterizing the ratio of magnetic and elastic forces is introduced according to the relation

$$\mathrm{Cm} = \frac{2\pi\chi^2 H_0^2 \pi a^2 L^2}{(\mu+1)C}.$$

On the basis of Eqs. (11) and (12) in Ref. [10], the dynamics of the free rod in the rotating magnetic field have been studied. In the case of the rod with one end fixed, the boundary conditions necessary for the solution of the set of Eqs. (11) and (12) are a bit less trivial. To deduce these, Eq. (11) is multiplied by $-\sin\vartheta\vec{e}_x$ and $\cos\vartheta\vec{e}_y$ and the obtained results are added. Then, accounting for the condition of the inextensibility, we obtain

$$\frac{\partial}{\partial l}\frac{\partial\vec{r}}{\partial t} = \frac{\partial}{\partial l}\vec{v}$$

and after integrating

$$\frac{\partial\vec{r}}{\partial t} = \frac{1}{\zeta}\vec{K}. \tag{13}$$

Thus, the boundary conditions for the set of Eqs. (11) and (12) compatible with the condition of the fixed end at $l=-1$ is

$$\vec{K}(-1) = \vec{0}. \tag{14}$$

The boundary condition corresponding to the clamped end of the rod is

$$\vartheta(-1) = 0. \tag{15}$$

For the free end we have

$$\frac{d\vartheta}{dl}(+1) = 0, \tag{16}$$

and

$$\vec{F}(+1) = F_a\vec{e}_y, \tag{17}$$

where F_a is applied force scaled with respect to C/L^2.

In the case of the small deformation of the rod, Eqs. (11) and (12) can be considerably simplified. In this case, since $\Lambda=0$ up to the second order small term, Eq. (11) reads

$$\vartheta_t = -\vartheta_{llll} + 2\ \mathrm{Cm}\ \vartheta_{ll}. \tag{18}$$

Introducing $\vartheta = y_x$ for the displacement of the rod y after integrating Eq. (18) once we have

$$y_t = -y_{xxxx} + 2\ \mathrm{Cm}\ y_{xx}. \tag{19}$$

The solution of Eq. (19) with boundary conditions corresponding to the semi-infinite rod

$$-y_{xxx}(0) = F_a,$$

$$y_{xx}(0) = 0,$$

$$y(-\infty) = 0, \tag{20}$$

and initial condition $y(x,0)=0$ can be easily found by Laplace transformation. In the case $\mathrm{Cm}=0$, the solution reads

$$y(x,t) = \frac{1}{2\pi i}\int_{\gamma-i\infty}^{\gamma+i\infty}\frac{e^{pt}\sqrt{2}F_a e^{/1\sqrt{2}p^{1/4}x}}{p^{7/4}}\cos\left(\frac{1}{\sqrt{2}}p^{1/4}x\right)dp.$$

Finding the inverse transform for $x=0$ we have

$$y(0,t) = \frac{F_a\sqrt{2}\ t^{3/4}}{\Gamma(7/4)}. \tag{21}$$

The result given by relation (21) is used for the testing of the numerical simulation results of the rod dynamics. The solution of Eq. (19) at $\mathrm{Cm} \neq 0$ is more complex.

For the displacement of the end of rod in this case we have

$$y(0,t) = \frac{1}{2\pi i}\int_{\gamma-i\infty}^{\gamma+i\infty} \times e^{pt}\frac{2iF_a\sqrt{p-\mathrm{Cm}}}{p^2[(\mathrm{Cm}+i\sqrt{p-\mathrm{Cm}})^{1/2}-(\mathrm{Cm}-i\sqrt{p-\mathrm{Cm}})^{1/2}]}dp. \tag{22}$$

III. NUMERICAL SIMULATION RESULTS

Equations (11) and (12) with boundary conditions (14)–(17) are solved by the numerical algorithm described in Refs. [7,10]. For the testing of the numerical simulation results the integral balance conditions for forces and torques have been checked. Integrating relation (13) along the rod and taking into account that $\vec{K}=d\vec{F}/dl$ gives the following condition of the force balance:

$$F_a\vec{e}_y = \vec{F}(-1) + \int \frac{\partial \vec{r}}{\partial t}dl.$$

Similarly for the torque balance we have

$$\int \vec{r}\times\frac{\partial \vec{r}}{\partial t}dl = \int \vec{r}\times\frac{d\vec{F}}{dl}dl = \vec{r}(+1)\times F_a\vec{e}_y - \int [\vec{t}\times\vec{F}]dl. \tag{23}$$

The last relation accounting for the torque balance Eq. (8) gives

$$[\vec{r}(+1)\times F_a\vec{e}_y] + \int \vec{T}_0 dl - \vec{M}(0) - \int \vec{r}\times\frac{\partial \vec{r}}{\partial t}dl = \vec{0}.$$

In the steady case, Eq. (19) for $\mathrm{Cm}=0$ at the boundary conditions at the free end $-y_{xxx}(1)=F_a$ and $y_{xx}(1)=0$ and boundary conditions at the fixed and clamped end $y(-1)=0$; $y_x(-1)=0$ has the following solution[6]:

$$y = F_a(x+1)^2 - \frac{F_a(x+1)^3}{6}, \tag{24}$$

which works for a small deformation of the rod. Relation (24) was used for interpretation of the experimental results in Ref. [6].

In Ref. [6] the bending of the flexible chain of the magnetic particles linked by the polymer molecules was studied by applying the force to its free end by the laser tweezer. By matching the experimentally observed shape of the rod with the theoretical curve (24) in Ref. [6], the curvature elasticity constant C has been determined. Since the experimental results are interpreted without taking into account normal force

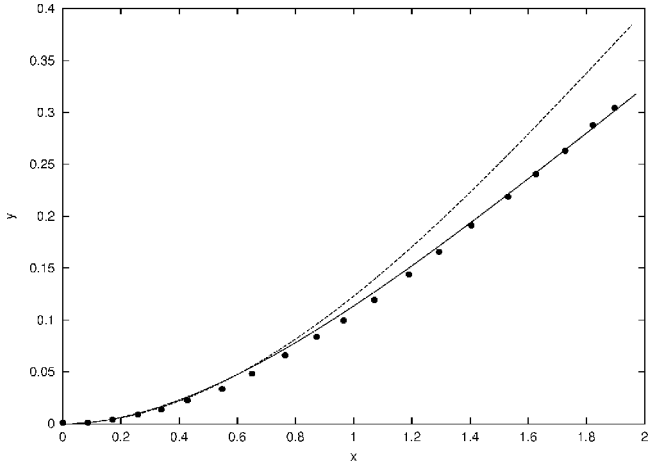

FIG. 1. Bending deformation of flexible magnetic chain. Numerical simulation results $F=0.15$; $\mathrm{Cm}=0$ (dashed line), $F=0.45$; $\mathrm{Cm}=0.9$ (solid line), experimental data of Ref. [6] for the PEG 733 linked chain are shown by filled circles.

F_n', which diminishes the deformation of the rod, overestimated curvature elasticity constant is obtained. To illustrate this point, in Fig. 1 together with the experimental data [6], the shapes of the flexible magnetic rod established in numerical simulation of the rod dynamics at $F=0.15$ and $\mathrm{Cm}=0$ and $F=0.45$ and $\mathrm{Cm}=0.9$ are shown. We see that the experimental data shown in Fig. 5 of Ref. [6] for the chain linked with polyethylene glycol with molecular weight 733 (PEG 733) can be reasonably well described by our model of flexible magnetic rod, but with a three times larger dimensionless force as we would have without taking into account the normal force. This gives an explanation as to why the elasticity constant of the PEG 733 chain obtained in the bending experiment is three times larger as found by buckling instability in Ref. [6]. The value of the magnetoelastic number $\mathrm{Cm}=0.9$ matching the experimental data allows one to estimate the magnetic permeability of the PEG 733 linked magnetic particles, which according to the technology of the preparation have a sandwichlike structure. Due to this, the magnetic susceptibility of the particles is not large and can be calculated according to the formula

$$(\mu-1)^2 = \frac{16CmC}{H_0^2a^2L^2}. \tag{25}$$

Taking for C the value 1.1×10^{-12} dyn cm^2 found by the buckling experiment of Ref. [6], a radius of particle $a=0.39$ μm, length of the chain $2L=41.2$ μm and a magnetic field strength of $H_0=300$ Oe for the magnetic permeability of the particles, we have $\mu=1.16$. This value seems to be reasonable for the magnetic particles used in experiments Ref. [6]. It should be noted that the value of magnetic permeability found gives some average magnetic property of the chain, which evidently depends on the distance between particles determined by the linker molecules. In agreement with this is the fact that the values of magnetic permeabilities found for PEG 733 and PEG 3400 linked chains are different and the higher value of magnetic permeability corresponds to

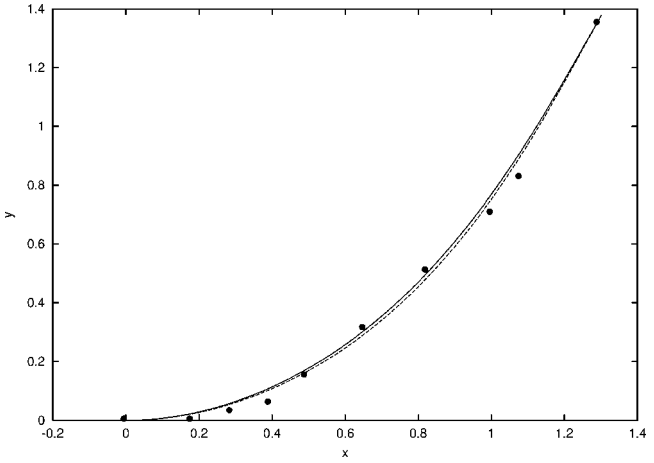

FIG. 2. Bending deformation of flexible magnetic chain. Numerical simulation results $F=1.1$; $\mathrm{Cm}=0$ (dashed line), $F=1.6$; $\mathrm{Cm}=0.33$ (solid line), experimental data of Ref. [6] for the PEG 3400 linked chain are shown by filled circles.

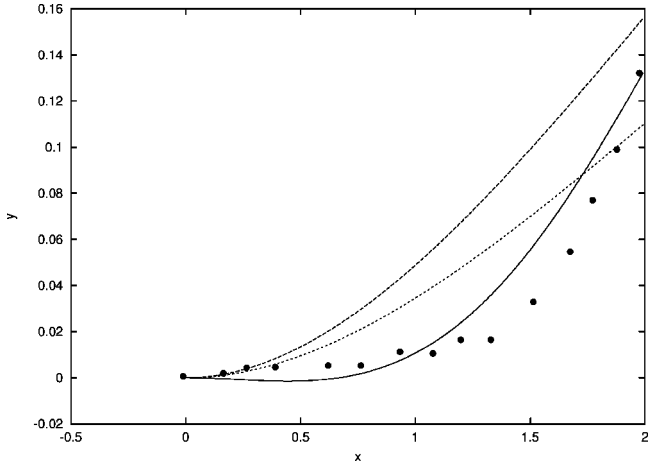

FIG. 3. Bending deformation of flexible magnetic chain. Numerical simulation results $F=0.06$; $\mathrm{Cm}=0$ (steady configuration, long dashed line); $F=0.04$; $\mathrm{Cm}=0$ (steady configuration, short dashed line); $F=0.5$; $\mathrm{Cm}=0$; $t=0.0972$ (nonrelaxed shape, solid line), experimental data of Ref. [6] for glutaraldehyde linked chain are shown by filled circles.

a shorter linker molecule. The experimental data shown in Fig. 6 of Ref. [6] for chain linked with another polymer PEG 3400 and steady configurations found by the numerical simulation of the rod dynamics for two cases $F=1.1$; $\mathrm{Cm}=0$ and $F=1.6$; $\mathrm{Cm}=0.33$ are shown in Fig. 2. We see that the steady configuration found accounting for the magnetic normal force matches the experimental data very well as does the configuration found without an accounting for magnetic normal force. This illustrates the point why the elasticity constant found in Ref. [6] by the bending experiment is approximately 1.46 times larger than that found from the study of chain buckling under the compression. The value of the magnetic permeability found in this case according to the relation (25) taking $2L=25.6$ μm and for the elasticity constant the value $2.2.10^{-14}$ dyn cm^2 (see the discussion about this value below) is smaller and equal to 1.022. We will return to this estimate when considering the relaxation and buckling experiments with PEG 3400 linked chain.

The chains linked by glutaraldehyde are stiffer. We were able to match the chain shape shown in Fig. 9 of Ref. [6] assuming that the chain shown in this figure has not achieved its steady state. We see from Fig. 3 that nonsteady shape is established at $F=0.5$; $\mathrm{Cm}=0$ at dimensionless time $t=0.0972$ matches the experimental one quite well; at least better than the stationary shapes shown in Fig. 3 for $F=0.04$ and $F=0.06$. Due to a possible uncertainty of the situation we have not attempted to estimate the magnetic permeability for this case.

The next series of experiments described in Ref. [6] consisted of the chain relaxation dynamics when the bending force due to the optical trap was removed. Experimental data together with the numerical simulation results for the dynamics of the free end of the rod are shown in Figs. 4 and 5 for PEG 733 and PEG 3400 linked chains, respectively. The Cm values were taken equal to that found by matching the steady shapes of the chains at bending experiments. Matching the experimental data with our numerical simulation results allowed us to determine the characteristic chain relaxation time $\zeta L^4/C$, which in the two cases shown turned out to be equal to 5 s for PEG 733 and 3.8 s for PEG 3400 linked chains, respectively. The value of the elastic relaxation time found allows us to estimate the curvature elasticity constant of chains. If we take for the viscosity of the surrounding liquid the value 10^{-1} P, then for the PEG 733 linked chain, which is 41.2 μm long we have $C=0.9\times10^{-12}$ dyn cm^2, but for the PEG 3400 linked chain, which is 25.6 μm long we have 1.97×10^{-13} dyn cm^2. The value of the elasticity constant for the PEG 733 linked chain is close to that given in Ref. [6]. The value of the elasticity constant obtained for the PEG 3400 linked chain gives a larger value for the magnetic permeability of the particles 1.068 than obtained above. Concerning the relaxation dynamics of the magnetic chain, it is rather important to note that the magnetic field can significantly influence the relaxation dynamics. This can be illustrated by the study of the power law determining the free end dynamics in the field. The linear fit of the numerical data for

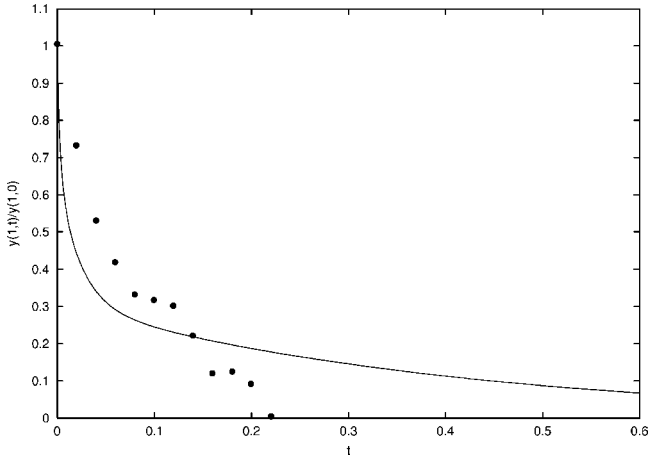

FIG. 4. Relaxation dynamics due to curvature elasticity. Numerical simulation results $F=0$; $\mathrm{Cm}=0.9$, experimental data of Ref. [6] for the PEG 733 linked chain are shown by filled circles.

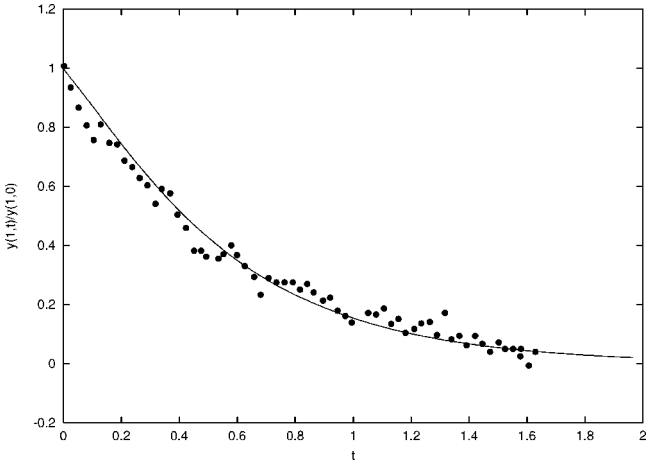

FIG. 5. Relaxation dynamics due to curvature elasticity. Numerical simulation results $F=0$; Cm=0.33, experimental data of Ref. [6] for the PEG 3400 linked chain are shown by filled circles.

the initial stage of the rod dynamics in semilogarithmic coordinates $\ln[y(+1)]=at+b$ at $F_a=0.15$ and Cm=0 gives $a=0.74$ and $b=-1.48$, which corresponds very well to the values found according to the theoretical relation (21). The characteristic power law $t^{3/4}$ experimentally is observed when studying the random Brownian motion of the passive Brownian particles in the mesh formed by flexible rodlike polymers [11,12]. It is interesting that the characteristic power law in the magnetic field is different. The dependence of the exponent for the free end dynamics on Cm found numerically is shown in Fig. 6. It would be interesting to follow this dependence by a study of the Brownian motion of passive bead in the mesh formed by the magnetic particle chains.

The third set of experiments described in Ref. [6] concerns the buckling instability of the chain arising under the action of compressional force. In the linear approximation when the tension in the rod Λ is constant and equal to the applied force, the equilibrium condition $K_n=0$ for the displacement of rod $y(x)$ reads

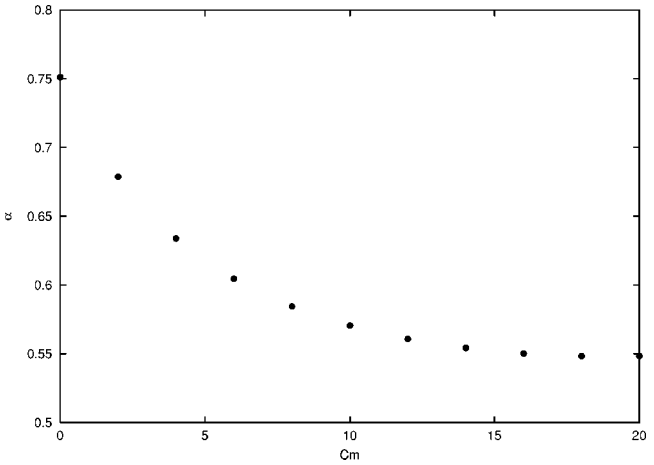

FIG. 6. Dependence of the power law of the free end dynamics on the magnetoelastic number Cm. Filled circles show numerical simulation data.

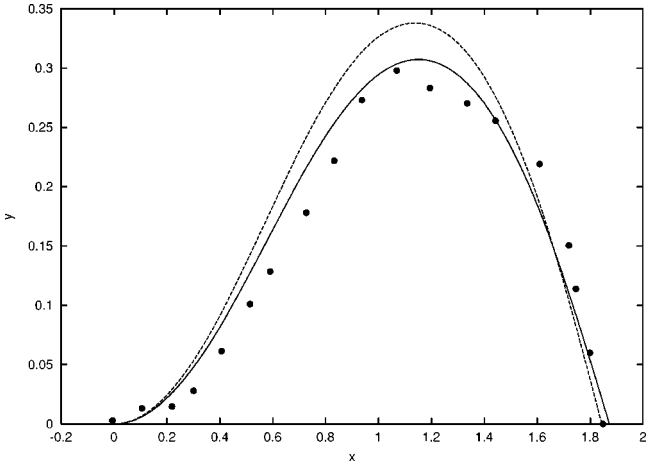

FIG. 7. Buckling instability of magnetic particle chain. Numerical simulation results $F_{\|}=4.4$; Cm=0.33 (solid line); $F_{\|}=4.4$; Cm =0.0 (dashed line), experimental data of Ref. [6] for the PEG 3400 linked chain are shown by filled circles.

$$-y_{xxxx}-\Lambda y_{xx}+2Cmy_{xx}=0. \tag{26}$$

The boundary conditions at free and fixed ends are $y_{xx}(+1)=0; y(+1)=0$ and $y_x(-1)=0; y(-1)=0$. Equation (26) at these boundary conditions gives the eigenvalue problem for the critical compression force $\Lambda=F_c$ in the following form:

$$\tan^{-1}(\sqrt{F_c-2\mathrm{Cm}})-\tan(\sqrt{F_c-2\mathrm{Cm}})=\frac{1}{\sqrt{F_c-2\mathrm{Cm}}}, \tag{27}$$

which for the critical compression force gives $F_c=2$ Cm $+2.247^2$. The corresponding eigenmode of the chain deformation is

$$y=(1-x)\sin\sqrt{F_c-2\mathrm{Cm}}+\frac{\sin[\sqrt{F_c-2\mathrm{Cm}}(x-1)]}{\cos\sqrt{F_c-2\mathrm{Cm}}}.$$

in the agreement with the experimental data [6] it describes the nonsymmetrical shape arising at the chain buckling. An interesting conclusion about the magnetic chain buckling is the dependence of the critical compressional force on the magnetoelastic number. Since the magnetic field strength was kept constant in the only existing experimental investigation [6], we do not have experimental verification of this at the present time. It is interesting to note that the increase of the critical force of the buckling instability with the charge of the flexible rod was found in Ref. [13].

We were able to match the shape arising due to the buckling instability, which was experimentally observed in Ref. [6], by the shape found from the numerical simulations. To carry out the numerical simulation we have kept the free end on the x axis. For this the force $F_{\perp}$ in y axis direction was also applied. Its magnitude was found by the Newton method solving the equation $y(+1,F_{\perp})=0$. Force along the x axis $F_{\|}$ was kept constant. The initial shape according to the found eigenmode of the chain deformation is given by

$$\vartheta = 0.15\left[\frac{\sqrt{F_c - 2\mathrm{Cm}}\,\cos[\sqrt{F_c - 2\mathrm{Cm}}(x-1)]}{\cos\sqrt{F_c - 2\mathrm{Cm}}} - \sin\sqrt{F_c - 2\mathrm{Cm}}\right].$$

The numerical simulation results for the steady shape of flexible rod at $\mathrm{Cm}=0.33$ and compressional force $F_{\parallel}=4.4$ are shown in Fig. 7. The value of $F_{\perp}$ found for steady configuration is 2.53. We see that the configuration found matches the shape experimentally observed in Ref. [6] rather well. To illustrate the magnetic field effect in Fig. 7 the shape of the rod for the same compressional force $F_{\parallel}$ but $\mathrm{Cm}=0$ is shown. We see that the application of the magnetic field diminishes the buckling of the rod. The value of dimensionless force 5.08 found for the buckling deformation matching the experimentally observed shape and the value of the force 2.2 pN applied by the laser tweezer allows us to estimate the curvature elasticity constant of the PEG 3400 linked chain $C=4.09\times10^{-14}$ dyn cm^2. This value and the value of the magnetoelastic number $\mathrm{Cm}=0.33$ for the magnetic permeability of the chain with length $2L=19.43$ μm gives 1.041—a value slightly larger than found from the bending experiments.

IV. CONCLUSION

We have shown by analytical and numerical investigations that the model of inextensible flexible magnetic rod describes rather well the existing experimental data for the chains of paramagnetic particles linked with different polymers. Accounting for the force normal to rod arising at the deformation of the magnetic chain in the applied field leads to several predictions—dependence of the threshold for buckling transition on the magnetic field strength, dependence of the chain deformation rate on the magnetic field strength, and others, which may be verified in future experiments. Rather interesting is the possibility of applying the model of flexible magnetic rod for the determination of the elastic properties of the linker molecules.

ACKNOWLEDGMENT

This work was supported by Grant No. LU 3 of University of Latvia.

[1] S. Melle, G. G. Fuller, and M. A. Rubio, Phys. Rev. E **61**, 4111 (2000).
[2] S. Melle, O. G. Calderon, M. A. Rubio, and G. G. Fuller, J. Non-Newtonian Fluid Mech. **102**, 135 (2002).
[3] S. Melle, O. G. Calderon, M. A. Rubio, and G. G. Fuller, Phys. Rev. E **68**, 041503 (2003).
[4] S. Melle and J. E. Martin, J. Chem. Phys. **118**, 9875 (2003).
[5] C. Goubault, P. Jop, M. Fermigier, J. Baudry, E. Bertrand, and J. Bibette, Phys. Rev. Lett. **91**, 260802 (2003).
[6] S. L. Biswal and A. P. Gast, Phys. Rev. E **68**, 021402 (2003).
[7] A. Cebers, J. Phys.: Condens. Matter **15**, S1335 (2003).
[8] L. D. Landau and E. M. Lifshitz, *Theory of Elasticity* (Nauka, Moscow, 1965).
[9] R. E. Goldstein, Th. R. Powers, and Ch. H. Wiggins, Phys. Rev. Lett. **80**, 5232 (1998).
[10] A. Cebers and I. Javaitis, Phys. Rev. E **69**, 021404 (2004).
[11] A. Caspi, R. Granek, and M. Elbaum, Phys. Rev. Lett. **85**, 5655 (2000).
[12] A. Caspi, R. Granek, and M. Elbaum, Phys. Rev. E **66**, 011916 (2002).
[13] R. Zandi, R. Golestanian, and J. Rudnick, e-print cond-mat/0308389.